Electron Spin Resonance, Optical, and Theoretical Studies of the Radical Anion of Sulfuryl Chloride[1]

Carolyn M. L. Kerr and Ffrancon Williams*

Contribution from the Department of Chemistry, University of Tennessee, Knoxville, Tennessee 37916.
Received November 11, 1971

Abstract: $SO_2Cl_2\cdot^-$ is the only observable product of electron attachment in γ-irradiated crystalline sulfuryl chloride at $-196°$. By contrast, $SO_2Cl_2\cdot^-$, $Cl_2\cdot^-$, and $SO_2\cdot^-$ have been identified by their esr spectra in γ-irradiated glassy solutions of sulfuryl chloride. The three species are readily distinguished by selective photobleaching, and this has been utilized in assigning an absorption band at 432 nm (λ_{max}) to $SO_2Cl_2\cdot^-$. A similar absorption band is observed at 415 nm in crystalline sulfuryl chloride. The esr parameters of $SO_2Cl_2\cdot^-$ in the glasses, $A_{\parallel}(^{35}Cl) = 62.4$–$62.9$ G and $g_{\parallel} = 2.0058$–2.0060, are close to the corresponding values (64.1 G and 2.0055) determined in polycrystalline sulfuryl chloride. Although the perpendicular features are not well defined in the powder spectra, the large anisotropy of the chlorine hyperfine splitting has been demonstrated by use of an aligned crystalline sample. The calculated spin density in the chlorine p orbitals is incompatible with the structures proposed for other 33-valence electron radicals and a novel structure has been proposed for $SO_2Cl_2\cdot^-$. The unpaired electron is visualized as occupying a supramolecular orbital comprising the lowest unoccupied orbitals of essentially separate SO_2 and Cl_2 molecules. Iterative extended Hückel calculations support this model and yield, in addition, electron spin density distributions for the radical similar to that found experimentally.

Electron attachment to molecules or ions can be a dissociative or nondissociative process, resulting either in two separate fragments or in a single paramagnetic species in which the original bonding framework is retained.

Recently we reported[2] the formation of $SO_2Cl_2\cdot^-$ by electron capture in γ-irradiated crystalline sulfuryl chloride. The esr spectrum of $SO_2Cl_2\cdot^-$ indicates that this radical anion represents a situation intermediate between these two cases. Dissociation does not occur, but rather extensive changes do take place both in the positions of the atoms and in the bonding arrangement. The structure of $SO_2Cl_2\cdot^-$ can best be visualized as a radical anion complex of sulfur dioxide and chlorine, in which the unpaired electron is associated with the lowest unoccupied orbitals of both molecules, so that there is appreciable spin density on all five atoms.

As it was originally thought that this complex might owe its stability only to the rigidity of the crystal, experiments have been undertaken with solutions of sulfuryl chloride in tetrahydro-2-methylfuran (MTHF) and various other organic glasses. Here we present esr and optical data obtained for the species produced by electron capture in these γ-irradiated glasses. There is clear evidence for the formation of $SO_2Cl_2\cdot^-$, but $Cl_2\cdot^-$ and $SO_2\cdot^-$ are also formed in comparable amounts. These results suggest, firstly, that $SO_2Cl_2\cdot^-$ does have some intrinsic stability, and, secondly, that the states $SO_2 + Cl_2\cdot^-$, $SO_2Cl_2\cdot^-$, and $SO_2\cdot^- + Cl_2$ are closely related, as is implied by the structure proposed for the radical. This latter conclusion is borne out by extended Hückel calculations which, in addition, yield electron spin density distributions for the radical fairly close to that found experimentally by esr.

Experimental Section

Materials. Sulfuryl chloride (Matheson Coleman and Bell) was degassed on a vacuum line over anhydrous magnesium sulfate (Fisher Scientific Co.) by several freeze–pump–thaw cycles. The material was then distilled into breakseals and stored in the dark. In spite of these precautions, a yellow color, presumably due to chlorine, developed in the liquid. During sample preparation, to avoid contamination, at least twice as much sulfuryl chloride as required was distilled into the sample container and the excess, along with all observable color, distilled out again.

The following solvents were used as received: 3-methylpentane and methylcyclohexane from Matheson Coleman and Bell, *n*-butyronitrile from Eastman Organic Chemicals, and ethyl alcohol (Commercial Solvents Corp.). Ethyl alcohol was dried over barium oxide (Barium and Chemicals) and the others over anhydrous magnesium sulfate. Tetrahydro-2-methylfuran (MTHF), supplied by Eastman Organic Chemicals, was purified as described previously.[3] All were degassed before use.

Chlorine and sulfur dioxide obtained from the Matheson Co. were degassed on the vacuum line. The chlorine was used without purification, but sulfur dioxide was allowed to sit for 15 min over decolorizing charcoal, molecular sieves, and barium oxide in turn at $-40°$. This procedure failed to remove the chemical giving rise to a blue color and a multiline esr spectrum in the irradiated bulk material.

Preparation of Samples. Esr tubes were made of Suprasil quartz of i.d. nominally 4 mm for all glassy samples, and 4, 2, or 1 mm for crystalline sulfuryl chloride. Optical cells were of two types: 2 × 1 × 0.2 cm standard quartz for glassy samples, and 1 × 1 × 0.1 cm extruded Suprasil for crystalline sulfuryl chloride.

Polycrystalline and poorly oriented samples of sulfuryl chloride were prepared by shock cooling the sample tubes or cells to $-196°$. Better oriented samples were obtained by controlled slow cooling through the freezing point.

Solutions for esr studies were prepared by distilling solute and solvent into the tubes, and estimating the concentration from the liquid heights, measured either at room temperature (sulfuryl chloride) or below 0° (chlorine and sulfur dioxide). In the case of optical samples, the cells are not suited to this technique and the solute and solvent volumes were determined in graduated reservoirs before distillation into the cell. Concentrations are estimated to be accurate to about 10% of the stated value. After the solution components had been thoroughly mixed, glasses were prepared by shock cooling the samples in liquid nitrogen.

The following solutions (concentrations in mole per cent) were used in the esr work: sulfuryl chloride in 3-methylpentane (3%),

(1) (a) This research was supported by the U. S. Atomic Energy Commission under Contract No. AT-(40-1)-2968, and this is AEC Document No. ORO-2968-70; (b) presented at the 3rd Southeastern Magnetic Resonance Conference, Oak Ridge, Tenn., Oct 1971, paper D2.

(2) C. M. L. Kerr and F. Williams, *J. Amer. Chem. Soc.*, 93, 2805 (1971).

(3) J. Lin, K. Tsuji, and F. Williams, *ibid.*, 90, 2766 (1968).

methylcyclohexane (6%), *n*-butyronitrile (5%), ethyl alcohol (3%), and MTHF (4, 7, 16, 23%); chlorine in MTHF (12, 18, 40%); sulfur dioxide in MTHF (9, 15%). The optical samples used were sulfuryl chloride in MTHF (3%) and chlorine in MTHF (4%).

γ Irradiations. Irradiations were carried out at −196° in an AECL Gammacell-200 cobalt-60 source to total doses of 1–3 Mrads. Samples were kept in the dark during irradiation and subsequently handled in subdued light.

Esr Measurements. These were made at −196° with the samples contained in a dewar with an unsilvered tail section extending through the sensitive region of the cavity. The spectra were recorded on a Varian V-4502 spectrometer using either the standard (V-4531) or the dual (V-4532) sample cavity. Hyperfine splittings and *g* factors were determined in the latter, using the dual channel chart recorder (G-22A) to record the spectra of sample and standard simultaneously. The standard used to calibrate the field scale was a dilute aqueous solution of manganous nitrate (the total width of the Mn^{2+} spectrum is 475 G). The *g* factors were determined using the hydrogen atom spectrum as an internal standard and the relationship

$$g_1 = g_2\{1/(1 + g_2\beta\Delta H/h\nu)\}$$

where g, β, h, and ν have their usual connotations, and subscripts 1 and 2 refer to sample and hydrogen atoms, respectively. ΔH is the distance in gauss between the centers of the sample and hydrogen atom spectra after correction of the latter according to the Breit–Rabi formula. The microwave frequency, ν, was measured using a Systron-Donner 50-MHz counter (Model 1037) with transfer oscillator plug-in unit (ACTO Model 1255A). The hydrogen atom *g* factor was taken to be 2.0021, a compromise between the values 2.00223[4] and 2.0019[5] reported respectively in methane and silica. Hydrogen atoms in the esr tube certainly contribute as the signal is observed in all samples regardless of whether the irradiated compound contains hydrogen. The *g* factors for $SO_2\cdot^-$ were also determined using a solution of potassium nitrosodisulfonate (Fremy's salt) in saturated potassium bicarbonate as a standard, for which $a_{iso}(N)$ was taken as 13.1 G and *g* as 2.0055.[6]

The accuracy of the calibration can be gauged from the range 501–504 G found for the hydrogen atom hyperfine splitting in a variety of materials and the value of 2.0021 measured for the hydrogen atom *g* factor in a sulfuryl chloride–MTHF glass using a solid mixture of diphenylpicrylhydrazyl (DPPH) in sodium chloride (g = 2.0036) as a standard. Taking into account both experimental and possible calibration errors, the estimated error in the hyperfine splittings obtained in this work is ±0.5 G and in the *g* factor ±0.0006.

The dual cavity was also used to monitor the signal intensity during quantitative photobleaching experiments. DPPH was used as the standard. Photobleaching of esr samples was carried out *in situ* using a 1000-W tungsten filament lamp to provide either white light with wavelengths covering the whole visible range (unfiltered) or red light of wavelength greater than 640 nm (using a Corning 2030 filter).

Optical Measurements. Uv and visible spectra were measured at −196° using a Cary-14 recording spectrophotometer equipped with an optical dewar similar in design and operation to one which has been described in detail elsewhere.[7] Photobleaching was carried out *in situ* using the unfiltered or filtered beam from the IR-2 lamp of the spectrophotometer as described above. Spectra were also recorded after melting and refreezing the samples for which removal from the dewar was necessary.

Results

Introduction. The results have been organized so as to emphasize the chemistry of the system rather than the methods of investigation. First, we describe the esr studies that have been used to identify $Cl_2\cdot^-$, $SO_2Cl_2\cdot^-$, and $SO_2\cdot^-$ and to investigate the initial distribution with which these species are formed as a result of electron capture by sulfuryl chloride. The selective photobleaching that was used as an aid in making the esr assignments involves interconversion of the radical anions, and these reactions have been examined by esr. In the next section, the results have been utilized in identifying the optical absorption spectra of $Cl_2\cdot^-$ and $SO_2Cl_2\cdot^-$. Following this, we turn to a closer examination of the esr spectrum of $SO_2Cl_2\cdot^-$ in crystalline sulfuryl chloride. This leads to an evaluation of the esr parameters and their implications with regard to structure. An unusual structure with a novel type of bonding has been proposed for $SO_2Cl\cdot^-$ and we conclude with a theoretical study of this model.

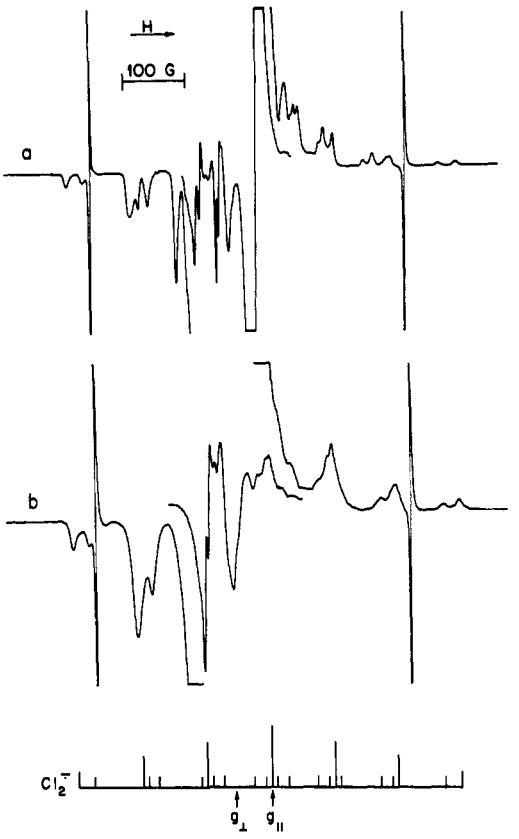

Figure 1. Esr first-derivative spectra of (a) γ-irradiated 16% SO_2Cl_2–MTHF glass at −196° showing $Cl_2\cdot^-$, $SO_2Cl_2\cdot^-$, and $SO_2\cdot^-$, and (b) γ-irradiated 40% Cl_2–MTHF glass at −196° showing $Cl_2\cdot^-$. In both spectra, the gain for the inner portions was attenuated by a factor of 5. The irradiation dose was *ca.* 1.5 Mrads in each case.

Esr Assignments of $Cl_2\cdot^-$ and $SO_2Cl_2\cdot^-$. Similar esr spectra were obtained after γ irradiation of sulfuryl chloride in all the aprotic glasses (MTHF, 3-methylpentane, methylcyclohexane, and *n*-butyronitrile). As will be discussed in detail later, the outer features of the representative spectrum shown in Figure 1a can be analyzed in terms of two distinct species, each containing two chlorines which are equivalent and have axially symmetric hyperfine tensors. The complexity of the pattern for each species is a result of the existence of two isotopes of chlorine. As the relative abundance of ^{35}Cl and ^{37}Cl is ≈3:1, only the $^{35}Cl^{35}Cl$ and $^{35}Cl^{37}Cl$ combinations contribute appreciably, the former giving rise to seven equally spaced lines with relative intensities 1:2:3:4:3:2:1 and the latter to sixteen lines of equal intensity and spacing dictated by $A_\parallel(^{37}Cl) \approx (5/6)\cdot A_\parallel(^{35}Cl)$.

The outermost parallel features in Figure 1a are free from overlap and can clearly be seen to correspond with

(4) R. W. Fessenden and R. H. Schuler, *J. Chem. Phys.*, **39**, 2147 (1963).
(5) S. Ogawa and R. W. Fessenden, *ibid.*, **41**, 1516 (1964).
(6) C. M. L. Kerr, Ph.D. Thesis, University of Aberdeen, Scotland, 1970.
(7) W. H. Hamill in "Radical Ions," E. T. Kaiser and L. Kevan, Ed., Wiley, New York, N. Y., 1968, Chapter 9, p 321.

Table I. Esr Parameters of $Cl_2\cdot^-$ in Various Matrices[a]

System	$A_\parallel^{35}$	$A_\parallel^{37}$	$A_\parallel^{35}/A_\parallel^{37}$ [b]	$g_\parallel$	$g_\perp$
SO_2Cl_2–3-methylpentane	103.1			2.0017	
SO_2Cl_2–methylcyclohexane	103.1			2.0017	
SO_2Cl_2–*n*-butyronitrile	103.6	86.0	1.204	2.0021	
SO_2Cl_2–MTHF	103.6	86.4	1.200	2.0019	
Cl_2–MTHF	103.9	86.5	1.201	2.0017	2.0383
H_2O_2–LiCl glass[c]	103 ± 1			2.004	2.050
Na–Cl_2 in H_2O, benzene, cyclohexane (polycrystalline)[d]	99–101			2.0013–2.0036	2.0370–2.0372
KCl single crystal[e]	101.4			2.0010	2.0438

[a] Hfs in gauss. [b] Theoretical value 1.201. [c] E. Ben Zvi, R. A. Beaudet, and W. K. Wilmarth, *J. Chem. Phys.*, **51**, 4166 (1969). [d] Reference 8. [e] Reference 9; $g_\perp$ is the average of the two largest principal values.

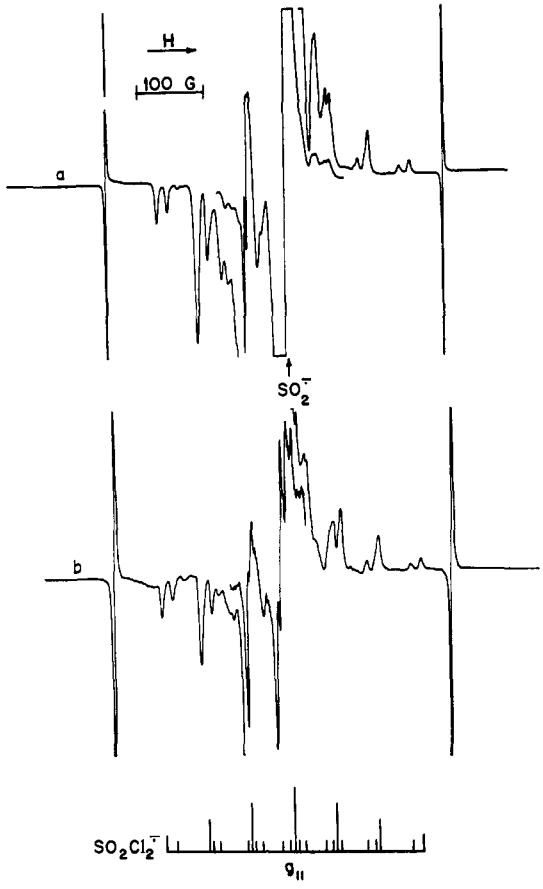

Figure 2. Esr first-derivative spectra of (a) γ-irradiated 16% $SOCl_2$–MTHF glass at −196° after photobleaching with red light showing $SO_2Cl_2\cdot^-$ and $SO_2\cdot^-$, and (b) γ-irradiated polycrystalline sulfuryl chloride at −196° showing $SO_2Cl_2\cdot^-$. The gains for the inner portions were attenuated by factors of 5 and 2, respectively

those in Figure 1b recorded for a γ-irradiated solution of chlorine in the same matrix (MTHF). These features are assigned to $Cl_2\cdot^-$ on the basis of the close similarity of the spectra and the esr parameters (Table I) to those obtained by other workers.[8] Selective photobleaching with red light removes $Cl_2\cdot^-$ cleanly from the γ-irradiated sulfuryl chloride solution, resulting in a simplification of the spectrum as shown in Figure 2a. By comparison with the spectrum of $SO_2Cl_2\cdot^-$ in γ-irradiated polycrystalline sulfuryl chloride (Figure 2b), the prominent outer components can be identified with the parallel features of $SO_2Cl_2\cdot^-$ and the relevant parameters are given in Table II.

Table II. Esr Parameters of $SO_2Cl_2\cdot^-$ in Various Matrices[a]

System	$A_\parallel^{35}$	$A_\parallel^{37}$	$A_\parallel^{35}/A_\parallel^{37}$ [b]	$g_\parallel$
SO_2Cl_2–3-methylpentane	62.7	52.3	1.198	2.0060
SO_2Cl_2–methylcyclohexane	62.8	52.5	1.196	2.0060
SO_2Cl_2–*n*-butyronitrile	62.9	52.3	1.204	2.0060
SO_2Cl_2–MTHF	62.4	52.2	1.196	2.0058
SO_2Cl_2 bulk polycrystalline[c]	64.1	53.3	1.203	2.0055

[a] Hfs in gauss. [b] Theoretical value 1.201. [c] Hfs taken from ref 2; $g_\parallel$ was wrongly quoted as 2.0050 in this work.

Returning to the spectrum in Figure 1a, it can be seen that the $m_I = \pm 2$ parallel features of $Cl_2\cdot^-$ are overlapped by the $m_I = \pm 3$ features of $SO_2Cl_2\cdot^-$. Here, in both the high- and low-field groups, only three lines are resolved as the inner $^{35}Cl^{37}Cl$ lines of $Cl_2\cdot^-$ are almost exactly superimposed on the two peaks in the $SO_2Cl_2\cdot^-$ spectrum. Although the intense $m_I = \pm 1$ features of $Cl_2\cdot^-$ also overlap the inner lines of the $m_I = \pm 2$ groups of $SO_2Cl_2\cdot^-$, the strong outer feature of the $m_I = +2$ manifold of $SO_2Cl_2\cdot^-$ is very well resolved. In addition, the intense $m_I = \pm 1$ lines of $SO_2Cl_2\cdot^-$ are almost free from overlap. There is, overall, a remarkable resemblance between the parallel features of the $Cl_2\cdot^-$ and the $SO_2Cl_2\cdot^-$ spectra, particularly in the sharpness of the $m_I = \pm 1$ groups and in the broadening of the high-field lines.

The perpendicular features, although theoretically more intense than the parallel, are not well defined for either $Cl_2\cdot^-$ or $SO_2Cl_2\cdot^-$. This is probably mainly due to a combination of quadrupole interactions and second-order effects which are known from single-crystal studies[9] to become very large near the perpendicular orientation. Both of these effects will cause an asymmetric broadening of the features in the powder spectrum, and this will be particularly marked because of the relatively small perpendicular ^{35}Cl hyperfine splittings which characterize $Cl_2\cdot^-$ ($A_\perp \approx 10$ G)[9] and $SO_2Cl_2\cdot^-$ ($0 < A_\perp < 16$ G), as determined from single-crystal measurements. The position of $g_\perp$ for $Cl_2\cdot^-$ indicated in Figure 1a corresponds to the feature chosen in a

(8) J. E. Bennett, B. Mile, and B. Ward, *J. Chem. Phys.*, **49**, 5556 (1968).

(9) T. G. Castner and W. Känzig, *J. Phys. Chem. Solids*, **3**, 178 (1957).

Table III. Esr Parameters of $SO_2\cdot^-$

System	g_1	g_2	g_3	g_{iso}
SO_2Cl_2–MTHF	2.0017	2.004	2.0118	2.0059
$K_2S_2O_5$ single crystal at 25° [a]	2.0019 ± 0.0020	2.0057 ± 0.0005	2.012 ± 0.003	2.0065
KCl single crystal at 25° [b]	2.0025 ± 0.0005	2.0071 ± 0.0005	2.0110 ± 0.0005	2.0066
$K_2S_2O_4$ aqueous solution at 25° [a]				2.0055 ± 0.0002

[a] A. Reuveni, Z. Luz, and B. L. Silver, *J. Chem. Phys.*, **53**, 4619 (1970). [b] J. Schneider, B. Dischler, and A. Raüber, *Phys. Status Solidi*, **13**, 141 (1966).

previous study[8] and this yields a value of 2.038 in close agreement with the range of 2.035–2.037 found for $Cl_2\cdot^-$ in a number of different polycrystalline matrices. However, since these results differ from the values of 2.044–2.046 determined in alkali halide single crystals,[9] it is possible that $g_\perp$ is not located exactly at the assigned peak position in the first-derivative powder spectrum. By analogy to the $Cl_2\cdot^-$ assignment, $g_\perp(SO_2Cl_2\cdot^-)$ may be signified by the corresponding central feature present in the spectrum of Figure 2a, in which case the $g_\perp$ factors for the two species coincide almost exactly.

For both $Cl_2\cdot^-$ and $SO_2Cl_2\cdot^-$, the data summarized in Tables I and II show that there is remarkably little variation of the esr parameters with the nature of the glassy matrix. In fact, we can probably conclude that within experimental error these parameters are independent of the solvent. For $Cl_2\cdot^-$, the $g_\parallel$ factors fall within the range covered by previously reported values, although the present hyperfine splittings appear to be slightly higher than previous results[8,9] obtained in ionic and molecular crystals. For $SO_2Cl_2\cdot^-$, we find that both the values of $g_\parallel$ and $A_\parallel$ (^{35}Cl) are slightly different in the glasses and the polycrystalline material; although these differences are small, they are thought to be real.

Esr Assignment of $SO_2\cdot^-$. The effects of progressive photobleaching on the central portion of the spectrum are shown in Figure 3. As discussed previously, photobleaching with red light removes $Cl_2\cdot^-$. From a comparison of the spectra in Figures 3a and 3b, this change does not affect the general shape of the central line, and this is consistent with the relatively low intensity in the center of the $Cl_2\cdot^-$ spectrum (Figure 1b). Additional photobleaching with unfiltered light removes the spectrum of $SO_2Cl_2\cdot^-$ and causes a large increase in the intensity of the center region, as shown in Figure 3c. The general appearance of this central line is indicative of a species with an anisotropic g factor but no hyperfine splitting and the line is therefore assigned to $SO_2\cdot^-$. There is good agreement between the measured g factors and recently published values, as shown in Table III. Although the spectrum of $SO_2\cdot^-$ only becomes clear on photobleaching $SO_2Cl_2\cdot^-$, the presence of $SO_2\cdot^-$ prior to this can be inferred from the greater intensity of the center line relative to the $m_I = +1$ component of $SO_2Cl_2\cdot^-$ in the spectrum of Figure 2a than in the spectrum of $SO_2Cl_2\cdot^-$ alone (Figure 2b). Furthermore, since the spectrum of $Cl_2\cdot^-$ contributes very little to the central feature, the similarity between this portion of the spectrum in Figures 3a and 3b indicates that $SO_2\cdot^-$ is also present initially.

An attempt was made to generate $SO_2\cdot^-$ independently by γ irradiation of SO_2–MTHF glasses. However, these samples yielded a singlet esr spectrum at higher magnetic field than the $SO_2\cdot^-$ signal. In addition, the glass was intensely blue, whereas the fully bleached SO_2Cl_2–MTHF glass was colorless. It appears that commercial sulfur dioxide contains some impurity, possibly sulfur trioxide, which acts as a highly efficient electron scavenger.

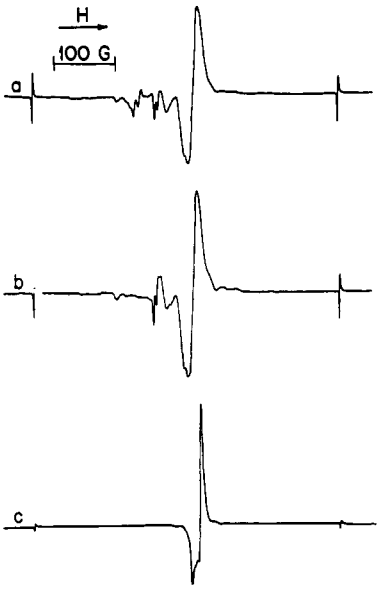

Figure 3. Esr first-derivative spectra of γ-irradiated 16% SO_2Cl_2–MTHF glass at −196° recorded at low gain to reveal center region (a) initially showing $Cl_2\cdot^-$, $SO_2Cl_2\cdot^-$, and $SO_2\cdot^-$, (b) after photobleaching with red light showing $SO_2Cl_2\cdot^-$ and $SO_2\cdot^-$, and (c) after photobleaching with white light showing $SO_2\cdot^-$. The gain in spectrum (c) was a factor of 5 less than in (a) and (b).

Esr Results in Ethanol Glasses. In contrast to the results obtained in aprotic glasses, no traces of $Cl_2\cdot^-$, $SO_2Cl_2\cdot^-$, or $SO_2\cdot^-$ were observed in γ-irradiated SO_2Cl_2–ethanol glasses. The glasses were colorless and the esr spectra provided evidence for the presence of the $CH_3\dot{C}HOH$ and $C_2H_5\cdot$ radicals, the latter in considerably smaller yield. A γ-irradiated ethanol glass containing no additive was purple and its esr spectrum was composed of the trapped electron singlet superimposed on the broad quintet from $CH_3\dot{C}HOH$.

Initial Ratio of $Cl_2\cdot^-$ to $SO_2Cl_2\cdot^-$. Although the esr spectra in the aprotic glasses are similar, there are definite differences in the relative amounts of $Cl_2\cdot^-$ and $SO_2Cl_2\cdot^-$ formed in each case. Before proceeding to consider these results, it can definitely be stated that the $Cl_2\cdot^-$ which is formed together with the $SO_2Cl_2\cdot^-$ does not originate from electron capture by traces of chlorine in the sulfuryl chloride samples. As mentioned in the Experimental Section, efforts were taken

Table IV. Initial Radical Anion Distribution and Effect of Photobleaching

System	Concentration of SO_2Cl_2, mol %	$[Cl_2\cdot^-]/[SO_2Cl_2\cdot^-]$	% increase in $[SO_2Cl_2\cdot^-]$ on red photobleaching
SO_2Cl_2–3-methylpentane	3	1.0	32
SO_2Cl_2–methylcyclohexane	6	1.05, 0.95	42
SO_2Cl_2–MTHF	4	0.60	27
SO_2Cl_2–MTHF	7	0.67	28
SO_2Cl_2–MTHF	16	0.51	32
SO_2Cl_2–MTHF	23	0.43	
SO_2Cl_2–*n*-butyronitrile	5	0.24	9
SO_2Cl_2 bulk polycrystalline	100	~0	

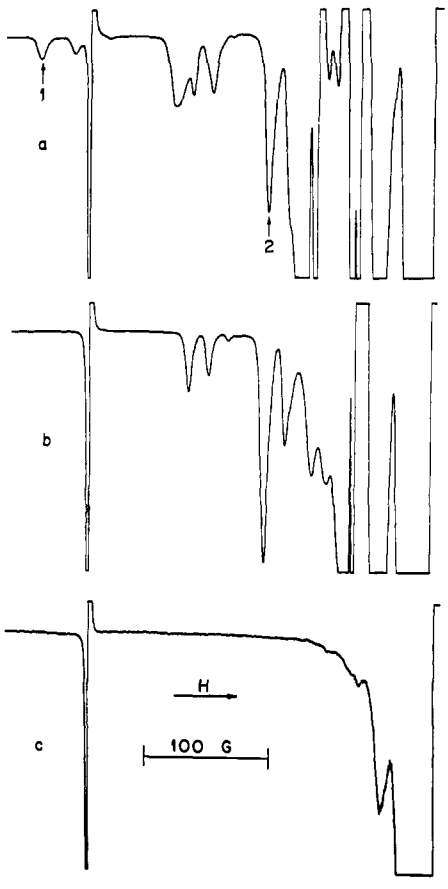

Figure 4. Low-field portions of esr first-derivative spectra corresponding to those described in Figure 3. The spectra in this figure were all recorded at the same gain.

to minimize the chlorine content during sample preparation so that the amount present was insignificant compared to the chlorine concentration required to produce a $Cl_2\cdot^-$ signal of corresponding intensity in the Cl_2–MTHF system. A qualitative estimate of the concentration ratio $[Cl_2\cdot^-]/[SO_2Cl_2\cdot^-]$ can be derived from the heights of corresponding lines ($^{35}Cl^{35}Cl$, $m_I = +3$). This was obtained from the relative intensities of the lines marked 1 and 2 in Figure 4a corrected by the ratio of the intensities of line 2 and the outermost low-field line in the $SO_2Cl_2\cdot^-$ spectrum of Figure 4b; as discussed earlier, line 2 originates solely from the $m_I = +2$ manifold of $SO_2Cl_2\cdot^-$. The concentration ratios obtained in this way are listed in Table IV. These values should be regarded as lower limits because the line width difference between the $m_I = +3$ components of the $Cl_2\cdot^-$ and $SO_2Cl_2\cdot^-$ spectra has been neglected (the latter is about 80% of the former). For each species, the line width is independent of the glass, and it is therefore thought that the variation in the observed ratios reflects some property of the solvent. There is some trend to a lower ratio as the sulfuryl chloride concentration is raised in the MTHF matrix, and almost no $Cl_2\cdot^-$ is formed in the polycrystalline sulfuryl chloride.

It would have been useful to ascertain the initial yield of $SO_2\cdot^-$ relative to that of $SO_2Cl_2\cdot^-$ and $Cl_2\cdot^-$, but this was rendered impossible by the overlap in the center region of the spectrum.

Esr Photobleaching Experiments. In addition to facilitating the spectral assignments, the photobleaching experiments also provide insight into the chemistry of the three radical anions in this system. When $Cl_2\cdot^-$ was removed with red light, there was a simultaneous increase in the $SO_2Cl_2\cdot^-$ signal intensity. The effect can be seen clearly in Figure 4 which shows the low-field portions of the spectra obtained from the γ-irradiated SO_2Cl_2–MTHF glass initially (a), after photobleaching with red light (b), and after photobleaching with white light (c). The increase in the $SO_2Cl_2\cdot^-$ signal can be measured from line 2 and the quantitative results for the various glasses are included in Table IV. Incidentally, for both the SO_2Cl_2–MTHF and the Cl_2–MTHF glasses, photobleaching of the $Cl_2\cdot^-$ was also accompanied by a clear increase in the signal intensity of the septet spectrum[10] from the solvent radical.

As noted previously, the removal of $SO_2Cl_2\cdot^-$ was always accompanied by a very marked increase in the $SO_2\cdot^-$ signal (Figures 3b and 3c). A semiquantitative analysis using double integration of the spectra suggests that the reaction represents conversion of $SO_2Cl_2\cdot^-$ to $SO_2\cdot^-$.

Optical Results in Glassy and Polycrystalline Samples. Studies of the optical absorption spectra were prompted by the pronounced effects of photobleaching on the esr spectra of glassy samples. In addition, the color of the γ-irradiated glassy samples (golden yellow) was quite different from that of the γ-irradiated crystalline sulfuryl chloride (emerald green).

After γ irradiation, both the Cl_2–MTHF and SO_2Cl_2–MTHF glasses showed strong absorption over most of the visible range. However, relying on the assignment from the corresponding esr studies, selective photobleaching by red light enabled the absorption spectra of $Cl_2\cdot^-$ to be obtained by subtraction in both glasses and these spectra are shown in Figure 5. The spectra (a) and (b) refer to the Cl_2–MTHF and SO_2Cl_2–

(10) D. R. Smith and J. J. Pieroni, *Can. J. Chem.*, **43**, 876 (1965).

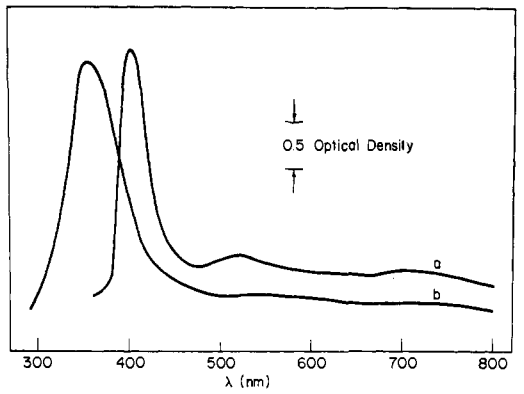

Figure 5. Optical absorption spectra at −196° of $Cl_2 \cdot^-$ (a) formed in γ-irradiated 4% Cl_2–MTHF glass, and (b) formed in γ-irradiated 3% SO_2Cl_2–MTHF glass. Both spectra were obtained by subtracting the spectrum after photobleaching with red light from that recorded initially. A correction was applied in case (b) for details of which see text.

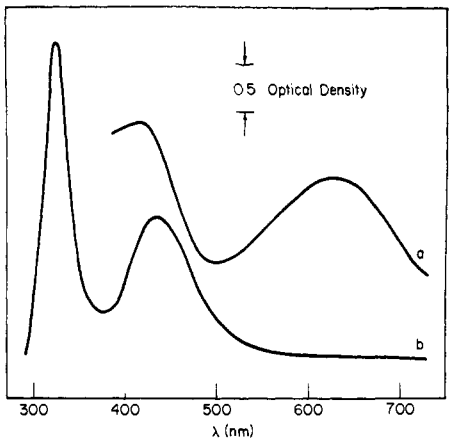

Figure 6. (a) Optical absorption difference spectrum of γ-irradiated polycrystalline sulfuryl chloride obtained from spectra recorded at −196° before and after melting the sample. (b) Optical absorption spectrum obtained at −196° from γ-irradiated 3% SO_2Cl_2–MTHF glass by subtracting the spectrum recorded after photobleaching with white light from that recorded after photobleaching with red light.

MTHF glasses, respectively. In the latter case, the absorption curve after red photobleaching was corrected for the increase in the $SO_2Cl_2 \cdot^-$ absorption (see later) according to the esr results in Table IV. The general contours of both spectra are similar, exhibiting a strong peak in the 400-nm region and additional weak absorption at longer wavelengths. These features closely resemble the optical absorption of $Cl_2 \cdot^-$ in X-ray irradiated potassium chloride[11] consisting of a strong band at 365 nm and a weak band at 750 nm, the latter having about $^1/_{60}$ of the intensity of the former. Therefore the assignment of the optical spectra in Figure 5 to $Cl_2 \cdot^-$ is corroborated. Interestingly, there is a definite shift in the wavelength at which the strong absorption band occurs in the two systems, the values of λ_{max} being 360 (SO_2Cl_2–MTHF) and 405 nm (Cl_2–MTHF).

Secondary photobleaching of the γ-irradiated SO_2Cl_2–MTHF glass with white light resulted in the subtraction spectrum (b) shown in Figure 6. Since the esr results show that $SO_2Cl_2 \cdot^-$ is removed in the glasses under these bleaching conditions, this optical absorption consisting of well-defined peaks at 325 and 432 nm can be similarly assigned, although we cannot rule out the possibility that part of the spectrum belongs to some extraneous species with the same photobleaching characteristics.

The absorption spectrum of γ-irradiated crystalline sulfuryl chloride is shown in Figure 6a. There was no photobleaching effect on this absorption, paralleling the esr results for $SO_2Cl_2 \cdot^-$ in the crystal. The optical spectrum in this case was obtained as the difference between absorption curves recorded at −196° before and after melting the sample. The steep rise in these absorption curves at low wavelengths due to light scattering by the polycrystalline sample precluded measurements for wavelengths below 370 nm. In keeping with the similarity between the corresponding esr spectra (Figure 2), the absorption maximum present at 415 nm in the crystal agrees reasonably well with the band at 432 nm assigned to $SO_2Cl_2 \cdot^-$ in the SO_2Cl_2–MTHF glass, considering the different media and the errors which may be introduced by the light scattering in the determination of λ_{max} for the former band. On the other hand, the peak at 630 nm in the crystal is completely absent in the glass so that it cannot be assigned to $SO_2Cl_2 \cdot^-$. This absorption is thought to arise from a cationic species in the sulfuryl chloride matrix which would certainly be absent in the SO_2Cl_2–MTHF glass. Some support for this tentative assignment comes from the observation that both the green color and the esr spectrum of $SO_2Cl_2 \cdot^-$ in the crystal disappeared simultaneously at −105°, suggesting the possibility of a charge neutralization process. This change was accompanied by the formation of another paramagnetic species, as yet unidentified.

In Table V we have summarized the values of λ_{max} for $Cl_2 \cdot^-$ and $SO_2Cl_2 \cdot^-$ obtained in this work together with the available results for $Cl_2 \cdot^-$ from the literature. The position of 405 nm for the strong band of $Cl_2 \cdot^-$ in the Cl_2–MTHF system appears to be outside the previously observed range of values for this absorption peak. Possible reasons for this anomaly will be discussed later. For $SO_2Cl_2 \cdot^-$, the short-wavelength peak at 325 nm in the glass could not be confirmed in the crystal spectrum because it lies outside the range of observation. Therefore this assignment is tentative.

Table V. Absorption Maxima for $SO_2Cl_2 \cdot^-$ and $Cl_2 \cdot^-$

System	Radical	λ_{max}, nm
SO_2Cl_2 bulk crystalline	$SO_2Cl_2 \cdot^-$	415 630[a]
SO_2Cl_2–MTHF	$Cl_2 \cdot^-$	360
	$SO_2Cl_2 \cdot^-$	325,[b] 432
Cl_2–MTHF	$Cl_2 \cdot^-$	405, 710
KCl[c]	$Cl_2 \cdot^-$	365, 750
H_2SO_4 glass[d]	$Cl_2 \cdot^-$	335

[a] For possible assignment see text. [b] Assignment based solely on photobleaching properties. [c] Reference 11. [d] D. M. Brown and F. S. Dainton, *Nature (London)*, **209**, 195 (1966).

Esr Spectra of $SO_2Cl_2 \cdot^-$ in Crystalline Sulfuryl Chloride. Hitherto the esr spectrum of $SO_2Cl_2 \cdot^-$ in the crystal has been discussed only by way of compari-

(11) C. J. Delbecq, B. Smaller, and P. H. Yuster, *Phys. Rev.*, 111, 1235 (1958).

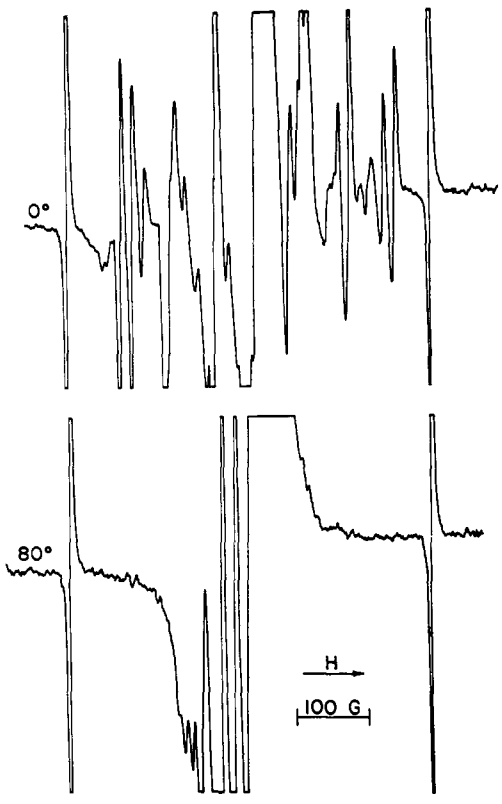

Figure 7. Esr first-derivative spectra of $SO_2Cl_2\cdot^-$ in a well-aligned sample of γ-irradiated crystalline sulfuryl chloride at $-196°$. The two spectra correspond to sample orientations differing by a rotation of 80° about the tube axis and were recorded at the same gain.

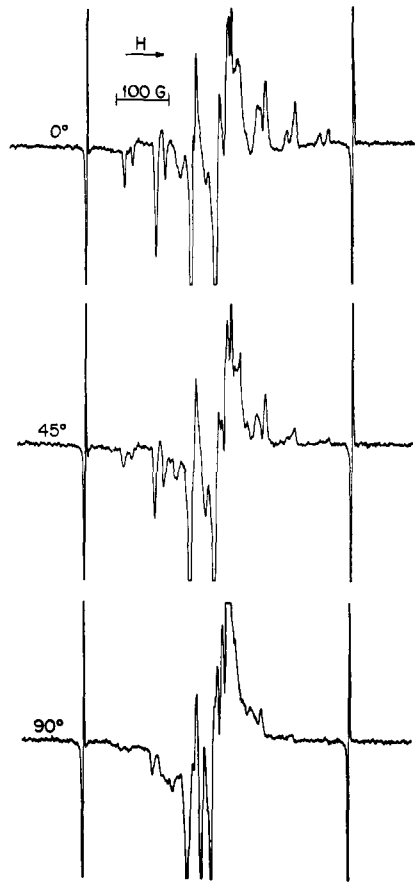

Figure 8. Esr first-derivative spectra of $SO_2Cl_2\cdot^-$ in a partly aligned sample of γ-irradiated crystalline sulfuryl chloride at $-196°$. The spectra refer to three different angles of orientation about the tube axis and were recorded at the same gain.

son with the results in the glasses. The polycrystalline spectrum (Figure 2b) is very similar to the spectrum in the MTHF glass (Figure 2a) and they are typical powder spectra as reflected by their line shapes and by the positional invariance of the spectral features with orientation of the sample. The large spread of the parallel features with no indication of perpendicular features in the outer regions of the spectrum suggests a high degree of anisotropy in the chlorine hyperfine splitting. This large anisotropy has been demonstrated qualitatively using well-aligned crystals of sulfuryl chloride. In Figure 7a, the sample orientation was chosen so that the spectral width is almost the same as in the polycrystalline sample but the first-derivative line shape is typical of an isotropic or single crystal spectrum. Rotation of the sample through 80° about the tube axis caused a considerable narrowing of the spectrum, as shown in Figure 7b. However, the lower limit for the hyperfine splitting could not be established from this experiment because of the buildup of intensity in the center of the spectrum with attendant loss of resolution.

Most spectra recorded in the literature fall into one or other of the two categories described above, *i.e.*, powder or single crystal spectra. However, an intermediate situation is sometimes found and esr results have been described[12,13] for samples exhibiting a small degree of preferential orientation. In this case,[12,13] the samples were prepared by the deposition of free radicals from the gas phase on cold surfaces, and alignment of radicals with respect to the surface was observed. A similar effect has been encountered during the course of work done in this laboratory on low-temperature methods for the preparation of aligned crystals from compounds which are liquids at room temperature.[14] The crystals are grown by slow cooling of the sample in esr tubes, and frequently only partial alignment is achieved by such techniques. Nevertheless, even a small degree of preferred orientation in the sample tube can be advantageous in certain circumstances and this is illustrated by the spectra in Figure 8. Relative to the intensity in the center of the spectrum, the parallel features are strongly enhanced in the upper 0° spectrum as compared to the spectrum of the randomly oriented sample in Figure 2b. In addition, the series of 0, 45, and 90° spectra shows a progressive weakening of the parallel features such that the $m_I = \pm 3$ lines are barely discernible in the 90° spectrum. On the other hand, the center region of the latter spectrum is greatly intensified and it is reasonable to conclude that the 90° spectrum emphasizes the perpendicular at the expense of the parallel features. There is a particularly large enhancement in the feature which is slightly off-center to low field. Previously, we tentatively associated this feature with $g_\perp$ and it coincides closely with the corresponding feature for $Cl_2\cdot^-$. Due to the general lack of resolution in the center of the 90°

(12) P. H. Kasai, W. Weltner, Jr., and E. B. Whipple, *J. Chem. Phys.*, 42, 1120 (1965).
(13) M. S. Wei, J. H. Current, and J. Gendell, *ibid.*, 52, 1592 (1970).
(14) (a) M. A. Bonin, K. Takeda, and F. Williams, *ibid.*, 50, 5423 (1969); (b) M. L. Bonin, M. A. Bonin, and F. Williams, *ibid.*, 54, 2641 (1971).

spectrum, the perpendicular hyperfine splitting cannot be measured but we can infer that the overall width of the perpendicular spectrum is less than 100 G, from which $A_\perp(^{35}Cl)$ lies between 0 and 16 G.

Structure of $SO_2Cl_2\cdot^-$. Information regarding the structure of $SO_2Cl_2\cdot^-$ can be deduced from the experimental esr parameters.[15,16] Assuming the hfs to be positive in sign with the values $A_\parallel(^{35}Cl)$ = 63.3 G (average for glasses and crystal) and $A_\perp(^{35}Cl)$ = 0–16 G, we obtain the limits for a_{iso} of 21.1 and 31.8 G and the corresponding values for $2B$ of 42.2 and 31.5 G. The magnitude of the isotropic coupling indicates only an insignificant spin density in the chlorine 3s orbitals, whereas the values of the anisotropic parameter $2B$ represent a spin density of 0.30–0.40 in a p orbital on each chlorine atom. In other words, well over half the total spin density is associated with the p orbitals on chlorine. This finding is incompatible with the models usually proposed for 33-valence electron radicals such as $SF_4\cdot^+$,[17] $POCl_3\cdot^-$,[18] and $PCl_4\cdot$,[19] in which the unpaired electron resides mainly on the central atom and the spin density on the ligands is usually of the order of 0.1. Supporting evidence against a central atom model is also furnished by the results for $PCl_2\cdot$[19] and α-substituted chloroalkyl radicals[20] where the anisotropy of the chlorine hyperfine splitting is much less than in the present case and arises from a small (<0.1) positive spin density in a p orbital on chlorine.

In proposing a structure for the $SO_2Cl_2\cdot^-$ species, two factors were taken into account. Firstly, as evidenced by Figures 1 and 2, there is a very marked resemblance between the esr spectra of $Cl_2\cdot^-$ and $SO_2Cl_2\cdot^-$ except for the difference in the hyperfine splittings; and secondly, both $SO_2\cdot^-$ and $Cl_2\cdot^-$ are well-known radical anions. The proposed structure, illustrated in Figure 9, can be rationalized in several ways, all of which emphasize the association of the unpaired electron with the combined SO_2 and Cl_2 moieties rather than with the integral SO_2Cl_2 molecule in which the S–Cl σ bonding is preserved. Thus SO_2Cl_2 can be thought of as a resonance hybrid of $SO_2\cdot^-$,Cl_2 and SO_2,$Cl_2\cdot^-$ or, equivalently, as a radical anion complex in which the two molecules share the unpaired electron. According to the molecular orbital representation in Figure 9, the unpaired electron occupies a supramolecular orbital derived from the lowest antibonding orbitals of SO_2 and Cl_2. A significant feature of this description is that the supramolecular orbital is compounded of orbitals which are antibonding between atoms in the individual molecules but are bonding between the molecules.

Theoretical Calculations. To justify the structure proposed for $SO_2Cl_2\cdot^-$, iterative extended Hückel calculations were carried out using a version of the method

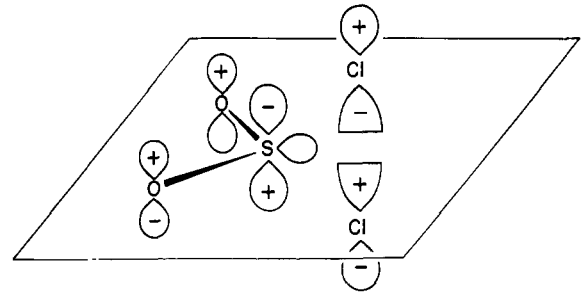

Figure 9. Supramolecular bonding orbital representation of $SO_2Cl_2\cdot^-$.

developed by Hoffmann.[21] In this the arithmetic mean formula

$$H_{ij} = 0.5KS_{ij}(H_{ii} + H_{jj})$$

is used for calculating off-diagonal matrix elements H_{ij}.[22] H_{ii} is the negative valence-state ionization potential of an electron in the ith orbital, S_{ij} is the overlap integral between the ith and jth orbitals, and K is an empirical constant. We have used Hinze and Jaffé's values for ionization potentials,[23] Slater AO's with the best atomic single ζ values given by Clementi and Raimondi,[24] and a value of 1.75 for K.[21]

Since it is recognized that this MO method does not always predict equilibrium geometries reliably,[21] the unpaired electron distributions were calculated for a variety of $SO_2Cl_2\cdot^-$ geometries and compared with the experimentally determined values. Only two configurations of the SO_2 fragment were used, corresponding to those in SO_2[25] and SO_2Cl_2[25] (S–O = 0.143 nm, $\angle$OSO = 120°) and $SO_2\cdot^-$[26] (S–O = 0.149 nm, $\angle$OSO = 110°). The Cl–Cl distance was varied over the range from 0.20 (bond distance in Cl_2[25]) to 0.33 nm (Cl–Cl distance in SO_2Cl_2), and the S–Cl distance over the range from 0.20 (S–Cl distance in SO_2Cl_2) to 0.365 nm (sum of S and Cl van der Waals radii[27]). The essential results are given in Table VI.

These results show that structures with geometries closely related to the SO_2Cl_2 molecule have unpaired electron distributions quite unlike that found experimentally. The same is true of the trigonal-bipyramid structure (although perhaps this result should be viewed with some reservation as the atomic orbital basis set did not include d orbitals). The chlorine p_z orbital spin densities are too low in both cases, as expected from the discussion in the previous section.

When the geometry of the system more closely resembles separate SO_2 and Cl_2 molecules, the spin density is almost entirely confined to the p_z orbitals of S, O, and Cl, as shown in the diagram of the proposed structure (Figure 9). For Cl–Cl distances near 0.20 nm, the lowest energy state can be represented as $SO_2\cdot^- + Cl_2$, as might be expected. As the Cl–Cl distance in-

(15) (a) P. W. Atkins and M. C. R. Symons, "The Structure of Inorganic Radicals," Elsevier, Amsterdam, 1967; (b) D. Schoemaker, *Phys. Rev.*, **149**, 693 (1966); (c) M. C. R. Symons, *Advan. Chem. Ser.*, **No. 88**, 1 (1968).

(16) The ^{33}S hfs parameters for $SO_2Cl_2\cdot^-$ would also be of considerable interest. Unfortunately, satellite lines from $^{33}SO_2Cl_2\cdot^-$ present in natural abundance (0.74%) could not be detected in this work because of low experimental sensitivity.

(17) R. W. Fessenden and R. H. Schuler, *J. Chem. Phys.*, **45**, 1845 (1966).

(18) C. M. L. Kerr and F. Williams, *J. Phys. Chem.*, **75**, 3023 (1971).

(19) G. F. Kokoszka and F. E. Brinckman, *J. Amer. Chem. Soc.*, **92**, 1199 (1970).

(20) (a) D. Pooley and D. H. Whiffen, *Spectrochim. Acta*, **18**, 291 (1962); (b) M. Kashiwagi, *Bull. Chem. Soc. Jap.*, **39**, 2051 (1966).

(21) (a) R. Hoffmann, *J. Chem. Phys.*, **39**, 1397 (1963); (b) P. C. Van Der Voorn and R. S. Drago, *J. Amer. Chem. Soc.*, **88**, 3255 (1966).

(22) M. Wolfsberg and L. Helmholz, *J. Chem. Phys.*, **20**, 837 (1952).

(23) J. Hinze and H. H. Jaffé, *J. Amer. Chem. Soc.*, **84**, 540 (1962).

(24) E. Clementi and D. L. Raimondi, *J. Chem. Phys.*, **38**, 2686 (1963).

(25) "Interatomic Distances," *Chem. Soc., Spec. Publ.*, **No. 11**, (1958).

(26) D. E. Milligan and M. E. Jacox, *J. Chem. Phys.*, **55**, 1003 (1971).

(27) L. Pauling, "The Nature of the Chemical Bond," 3rd ed, Cornell University Press, Ithaca, N. Y., 1960, p 260.

Table VI. Spin Density Distributions for Various Geometries of the $SO_2Cl_2\cdot^-$ System

Species	Distance, nm		Calculated spin densities[a-c]				
			Chlorine			Sulfur and oxygen	
	Cl–Cl	S–Cl	C^2_s	$C^2_{p_z}$	$C^2_{p_x}$	$\Sigma(C^2_s + C^2_{p_x} + C^2_{p_y})$	$\Sigma C^2_{p_z}$
d	0.33	0.20	0.050	0.158	0.027	0.495	0
e	0.44	0.22	0.004	0.133	0.030	0.674	0
$Cl_2 + SO_2\cdot^-$	0.20–0.22	>0.27	<0.001	<0.02	<0.02	0	>0.92
$SO_2Cl_2\cdot^-$ [f]	0.23	0.275–0.295	0.02–0.01	0.34–0.19	<0.01	0	0.26–0.59
$Cl_2 + SO_2\cdot^-$	0.23	0.305	0.007	0.109	0.008	0	0.753
$Cl_2 + SO_2\cdot^-$	0.23	>0.31	<0.003	<0.05	<0.007	0	>0.88
$Cl_2\cdot^- + SO_2$[g]	0.24	0.28–0.32	~0.02	>0.41	~0	0	<0.14
$Cl_2\cdot^- + SO_2$	0.25	>0.28	0.01–0.02	>0.47	~0	0	<0.03
$Cl_2\cdot^-$	0.28		0.005	0.495	0		
Experimental spin densities for $SO_2Cl_2\cdot^-$[h]			0.013–0.019	0.30–0.40	~0		

[a] The spin densities quoted are the averages of those obtained using the two SO_2 geometries described in the text. [b] The *z* direction is parallel to the chlorine internuclear axis. The *x* direction is perpendicular to the *z* axis in the ClSCl plane. [c] The total spin density has been taken as the sum of the net atomic orbital populations, neglecting overlap populations (*cf.* ref 21b). The value so obtained has been normalized to unity. [d] Geometry corresponds to that of neutral molecule. SO_2 geometry corresponding to $SO_2\cdot^-$ was not used in this calculation. [e] Geometry corresponds to a trigonal-bipyramid structure. [f] As represented in Figure 9. [g] For Cl–Cl = 0.24 nm and S–Cl > 0.32 nm, the spin density distribution represents either $SO_2 + Cl_2\cdot^-$ or $SO_2\cdot^- + Cl_2$ depending on whether SO_2 or $SO_2\cdot^-$ geometry is used in the SO_2 fragment. [h] Calculated assuming a_{iso} = 1680 G, $2B$ = 105 G for unit spin density in an s and a p orbital, respectively, of ^{35}Cl; a similar calculation gives $C^2_{p_z}$ = 0.58 for $Cl_2\cdot^-$ (ref 15c).

creases, a continuous variation in spin density from $SO_2\cdot^- + Cl_2$ (Cl–Cl = 0.20–0.22 nm) through $SO_2Cl_2\cdot^-$ (Cl–Cl = 0.23 nm, S–Cl = 0.275–0.295 nm) to $SO_2 + Cl_2\cdot^-$ (Cl–Cl = 0.24–0.25 nm) occurs. For Cl–Cl distances larger than this, convergence problems were encountered, and spin density distributions could not be obtained. The equilibrium distance for $Cl_2\cdot^-$ is predicted to be 0.28 nm. This value is regarded as significant only because the same set of calculations indicated a value (0.21 nm) very close to the experimental for the bond distance in Cl_2.

For geometries where Cl–Cl = 0.23 nm and S–Cl = 0.27–0.30 nm, the calculations predict appreciable spin densities on all five atoms, and the values for the p_z orbitals of chlorine are reasonably close to that found experimentally for $SO_2Cl_2\cdot^-$. The small or zero values for the other chlorine p orbitals imply axial symmetry of the chlorine hfs tensor which is consistent with the esr observations. The low-spin densities in the chlorine s orbitals are also encouraging as it is expected that most of the spin density in these orbitals arises through configuration interaction which the extended Hückel method does not take into account.

The results of the calculations show that the proposed structure is theoretically feasible and provide spin density distributions in acceptable agreement with the esr data. In addition, the very small range of atomic configurations which spans distributions corresponding to $SO_2\cdot^- + Cl_2$, $SO_2Cl_2\cdot^-$, and $SO_2 + Cl_2\cdot^-$ is in keeping with the formation of the three paramagnetic species $SO_2\cdot^-$, $SO_2Cl_2\cdot^-$, and $Cl_2\cdot^-$ in irradiated glassy solutions of SO_2Cl_2.

Discussion

In our preliminary communication,[2] we based the identification of $SO_2Cl_2\cdot^-$ solely on the esr results for polycrystalline sulfuryl chloride. Confirmation of this assignment is provided by the present work which demonstrates that $SO_2Cl_2\cdot^-$ is formed from sulfuryl chloride in a variety of γ-irradiated aprotic glasses. It is well established that in γ-irradiated glasses such as MTHF, where the positive charge is localized on a solvent molecule, this method is of general utility for producing anionic species from solutes by electron capture.[7] Another important result which emerges from this work is the observation of $Cl_2\cdot^-$ and $SO_2\cdot^-$ as well as $SO_2Cl_2\cdot^-$ in the glasses, although $SO_2Cl_2\cdot^-$ is the only product of electron capture in the crystal. Clearly, electron capture by sulfuryl chloride in these glasses involves competition between what may be formally regarded as a nondissociative process and two distinct dissociative paths. This situation is not often encountered with other solutes and clearly reflects the unusual nature of the $SO_2Cl_2\cdot^-$ radical anion.

None of the three radical anions were observed in ethanol glasses despite the evidence (absence of the characteristic trapped electron absorption) that electrons had been scavenged by the sulfuryl chloride. These results can be explained if proton transfer were to occur from the solvent to the radical anions immediately after their formation. Although no direct evidence was obtained for this process in the present case, analogous reactions have been established for aromatic radical anions in alcohol glasses.[28]

Returning to the process of electron capture, the observation of only $SO_2Cl_2\cdot^-$ in the crystal can perhaps be attributed to the rigidity imposed by a regular structure. Viscosity differences will not, however, explain the different relative quantities of $Cl_2\cdot^-$ and $SO_2Cl_2\cdot^-$ observed in the various glasses, since identical concentration ratios were obtained from 3-methylpentane and methylcyclohexane although the latter is known to be a harder glass at −196°. On the other hand, from the results listed in Table IV, the $[Cl_2\cdot^-]/[SO_2Cl_2\cdot^-]$ concentration ratio decreases with increasing solvent polarity (as indicated by their respective dipole moments[29]) and with increasing concentration of sulfuryl chloride in MTHF. The latter effect appears to be

(28) (a) T. Shida and W. H. Hamill, *J. Amer. Chem. Soc.*, **88**, 3689 (1966); (b) J. Lin, K. Tsuji, and F. Williams, *Trans. Faraday Soc*, **64**, 2896 (1968).

(29) (a) A. L. McClellan, "Tables of Experimental Dipole Moments," W. H. Freeman, San Francisco, Calif., 1963; (b) C. P. Smyth, "Dielectric Behavior and Structure," McGraw-Hill, New York, N. Y., 1955.

unrelated to polarity, as the dipole moments of sulfuryl chloride and MTHF are very similar,[29] and instead may be attributable to aggregation of sulfuryl chloride molecules at the higher concentrations. The influence of polarity implies that $SO_2Cl_2\cdot^-$, or its excited precursor, is stabilized by polar solvents. However, specific solvation does not appear to occur, as the esr parameters of $SO_2Cl_2\cdot^-$ are identical within experimental error in all the solvents (Table II).

The system under study provides an exceptionally clear example of how selective photobleaching can be used to differentiate between the spectra of trapped intermediates. It is also possible to correlate the optical absorption spectra of $Cl_2\cdot^-$ and $SO_2Cl_2\cdot^-$ in the glasses with the effects of excitation in different wavelength regions. Since the esr and optical studies have shown that $Cl_2\cdot^-$ is removed by red light (λ >640 nm), absorption in the weak band at *ca.* 710 nm is evidently responsible. This is consistent with the observation that physical effects (reorientation) are induced by photobleaching in the 750-nm band of $Cl_2\cdot^-$ in single crystals of potassium chloride.[11] On the other hand, $SO_2Cl_2\cdot^-$ is not bleached by red light and no absorption was detectable in this region. The removal of $SO_2Cl_2\cdot^-$ in the glasses by exposure to unfiltered visible light can be attributed to absorption in the 432-nm band.

Some comment is necessary on the discrepancy between λ_{max} for the strong bands in the spectra of $Cl_2\cdot^-$ in the Cl_2–MTHF and SO_2Cl_2–MTHF glasses. In the latter case, λ_{max} (360 nm) lies in the range (335–365 nm) found by other workers for $Cl_2\cdot^-$ in a variety of systems, whereas the value of λ_{max} in Cl_2–MTHF is 405 nm. It is thought that this is a consequence of the formation of a charge-transfer complex between chlorine and MTHF in the Cl_2–MTHF solution. Complexes between chlorine and ethers are well known,[30] and, during preparation of dilute Cl_2–MTHF solutions, it was noted that the yellow color faded within about 0.5 min of mixing and that the resulting glass was colorless. As MTHF would be the donor in the ground state, formation of $Cl_2\cdot^-$ would destroy the complex. The absence of $Cl_2\cdot^-$ complexing is evidenced by the fact that the esr parameters of $Cl_2\cdot^-$ in Cl_2–MTHF are not anomalous. However, the $Cl_2\cdot^-$ and MTHF molecules may remain in a favorable position for formation of an excited state complex which could be responsible for the observed shift. In the SO_2Cl_2–MTHF glass the $Cl_2\cdot^-$ is formed from SO_2Cl_2 and presumably is not correctly placed for formation of an excited state involving MTHF, so that a normal λ_{max} is observed.

The photobleaching experiments in the glasses have played a vital part in the identification of the radical anions but the reactions taking place during photobleaching in the SO_2Cl_2–MTHF system are an additional focus of interest. Definite evidence for interconversion of the radical anions during these reactions has been obtained. The removal of $Cl_2\cdot^-$ results in an increase of the $SO_2Cl_2\cdot^-$ concentration but the reaction is not quantitative. A concomitant increase occurs in the solvent radical concentration, and this is the only reaction which is observed when $Cl_2\cdot^-$ is photobleached in the Cl_2–MTHF system. In contrast, recent careful work[31] has shown that the photobleaching of trapped electrons in MTHF is accompanied by a significant decrease in the solvent radical concentration. Thus, it is unlikely that electrons are released from $Cl_2\cdot^-$ and the excited state probably dissociates to give chlorine atoms and chloride ions, a mechanism which has been suggested to explain the reorientation of $Cl_2\cdot^-$ in single crystals of potassium chloride during photobleaching.[11] The increase in solvent radical concentration can then be attributed to hydrogen atom abstraction by chlorine atoms. If electrons cannot migrate from $Cl_2\cdot^-$ to SO_2Cl_2 molecules, the interconversion to $SO_2Cl_2\cdot^-$ can be considered as a localized process involving the $Cl_2\cdot^-$ excited state and the neighboring SO_2 moiety.

The second photobleaching reaction appears to result in the conversion of $SO_2Cl_2\cdot^-$ to $SO_2\cdot^-$ with little or no increase in solvent radical concentration. Therefore the reaction most probably involves the elimination of a chlorine molecule, and this is consistent with the proposed structure of $SO_2Cl_2\cdot^-$.

In crystalline sulfuryl chloride, there is no observable photobleaching, even with uv light. Like the lack of formation of $SO_2\cdot^-$ and $Cl_2\cdot^-$ during γ irradiation, this is probably due to the rigidity of the crystal which would prevent the movement apart of the two fragments. Moreover, the crystal symmetry would be likely to preserve the C_{2v} symmetry of the system necessary for overlap of the sulfur, oxygen, and chlorine p_z orbitals, whereas the greater plasticity of the glass may facilitate torsional motion of the fragments. In this context, it is interesting that theoretical calculations indicate appreciable interaction between SO_2 and Cl_2 fragments can still occur at distances near the sum of the van der Waals radii of sulfur and chlorine.

Conclusions

The structure of $SO_2Cl_2\cdot^-$ provides the key to understanding the chemistry of the system described in this paper. Both the initial observation of the three radical anions and their interconversion during photobleaching are symptomatic of the close relationship between $Cl_2\cdot^- + SO_2$, $SO_2Cl_2\cdot^-$, and $Cl_2 + SO_2\cdot^-$. Theoretical calculations bear this out emphasizing that these three stable states of the system are encompassed by a small range of geometries. In spite of the intermediate character of $SO_2Cl_2\cdot^-$ implied by these results, the esr data definitely indicate that it is an integral chemical species. As such, it can be regarded as a radical anion complex, few examples of which have been reported to date.[32]

Acknowledgment. The authors wish to thank Dr. J. E. Bloor for his advice regarding the calculations and for allowing them to use his SCCMO program, a modified version of one obtained from Dr. R. S. Drago.

(30) R. S. Mulliken and W. B. Person, "Molecular Complexes," Wiley-Interscience, New York, N. Y., 1969, p 48.

(31) F. P. Sargent, *Can. J. Chem.*, **48**, 3453 (1970).

(32) *Cf.* E. D. Sprague, K. Takeda, and F. Williams, *Chem. Phys. Lett.*, **10**, 299 (1971).